THE JOURNAL OF
PHYSICAL CHEMISTRY C
Cite This: J. Phys. Chem. C 2019, 123, 3696−3702
Article
pubs.acs.org/JPCC

T−*P*−*X* Phase Diagram of the Water−Hydrogen System at Pressures up to 10 kbar

M. A. Kuzovnikov*[†,‡] and M. Tkacz[§]

[†]Institute of Solid State Physics RAS, 142432 Chernogolovka, Moscow District, Russia
[‡]Max Planck Institute for Chemistry (Otto Hahn Institute), Hahn-Meitner-Weg 1, 55128 Mainz, Germany
[§]Institute of Physical Chemistry PAS, Kasprzaka 44/52, 01-224 Warsaw, Poland

ABSTRACT: The stability field of the C_0 hydrogen hydrate in the pressure−temperature phase diagram of the water−hydrogen system is studied by volumetry under hydrogen excess. This stability field is confined by the sII hydrate stability field at the low-pressure side; by the liquid stability field at the high-temperature side; and by the C_1 hydrate stability field at the high-pressure side. The pressure of the $C_0 \leftrightarrow C_1$ phase equilibrium is temperature-independent in the studied temperature range from −20 to +18 °C. The corresponding equilibrium line in the phase diagram terminates at the nonvariant quadruple point "C_0 hydrate + C_1 hydrate + liquid H_2O + H_2 gas" (or Q_3) at 7.7(3) kbar and +22(2) °C. The volume change accompanying the $C_0 \rightarrow C_1$ phase transition, and the $\frac{dT}{dP_{H_2}}$ slopes of the melting lines of the C_0 and C_1 hydrates are measured by volumetry. Thermodynamic considerations are used to estimate the hydrogen content $H_2/H_2O \approx 0.53(5)$ and 0.23(5) of the C_0 and C_1 hydrates, respectively, near the Q_3 point.

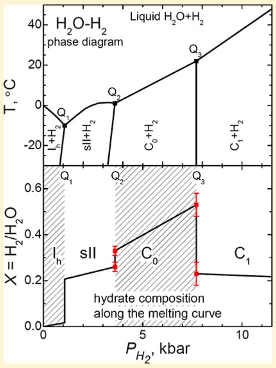

1. INTRODUCTION

Water ice and hydrogen are among the basic building materials of many planets and satellites. Therefore, the phase transformations of ice and the hydrogen effect on these transformations may play a key role in the evolution and interior structure of icy celestial bodies.[1]

Apart from dissolving in water ices, various gases can form distinct compounds with H_2O. Such compounds are called gas hydrates, and they belong to the rich family of clathrates, in which the host species (H_2O in our case) forms a strong tetrahedrally bonded framework with cages.[2] The guest molecules enter such cages, but only weakly interact with the host framework. H_2O molecules in gas hydrates and ices are bonded together by the hydrogen bonds so that the so-called "ice rules" are satisfied, with the interaction with guest molecules being the van der Waals one.

Unlike hydrates of most gases, which readily form at the pressure of few tens of bars,[2] hydrogen hydrates were not known for a long time because of much higher pressures needed for their formation. Only in 1993 did Vos et al.[3] make the first observation of the hydrate formation in the water−hydrogen system in the pressure interval 7.5−300 kbar. Two crystalline hydrogen hydrates were discovered: a rhombohedral C_1 hydrate (hydrogen filled ice II), stable at pressures up to 25.5 kbar, and a cubic C_2 hydrate (hydrogen filled ice I_c), stable at higher pressures. The composition of these phases was estimated on the basis of Raman spectroscopy and visual observations. The molecular ratio $X = H_2/H_2O$ of the C_1 hydrate between 7.7 and 25.5 kbar was found to be $X_{C_1} = 1/6$ (or 1.8 wt % H_2), and that of the C_2 hydrate was $X_{C_2} = 1$ (or 10 wt % H_2).[3]

Later, in 1999, Dyadin et al.[4] measured the melting curve of ices in a hydrogen atmosphere by differential thermal analysis at pressures up to 8 kbar and discovered another clathrate hydrate at hydrogen pressures from 1 to 3.6 kbar. In 2002, Mao et al.[5] identified the crystal structure of this hydrate, called sII, as a type 2 clathrate with a cubic unit cell containing 136 H_2O molecules. This hydrate has a nonstoichiometric nature and, depending on the temperature and pressure, up to 48 molecules of hydrogen (or 3.8 wt % H_2) can enter the host H_2O structure.[5,6] The *T*−*P* boundaries of the stability field of this hydrate were constructed[6,7] previously.

Recent studies on quenched and recovered to ambient pressure samples revealed new hydrogen hydrate, called C_0, at the intermediate pressure region between the sII and C_1 hydrates.[8] X-ray[8−11] and neutron[12,13] diffraction studies on the C_0 hydrate demonstrated that its crystal structure presents a clathrate of a new type. Similar hydrate was later found in the CO_2−H_2O system under high pressure.[13] A discovery of a new structural type of clathrate stimulated a series of theoretical works.[14−16]

The complete pressure−temperature phase diagram of H_2O under hydrogen pressure should include the stability field of the C_0 hydrate. The melting curves of solid phases were previously studied,[4] and the monovariant ternary "sII hydrate + C_0 hydrate + H_2 gas" and "liquid H_2O + C_0 hydrate + H_2 gas" equilibria (further referred to as the sII ↔ C_0 and C_0 ↔ L phase transition lines) were located earlier.[7] In this paper, we report on the volumetric in situ study of the hydrogen−water system, which

Received: December 16, 2018
Revised: January 15, 2019
Published: January 22, 2019

DOI: 10.1021/acs.jpcc.8b12083
J. Phys. Chem. C 2019, 123, 3696−3702

allowed us to locate the monovariant ternary "C_0 hydrate + C_1 hydrate + H_2 gas" equilibrium, further referred to as the $C_0 \leftrightarrow C_1$ phase transition line, thus completing the construction of the phase diagram of H_2O under up to 10 kbar pressure of hydrogen.

Hydrogen molecules can be removed from the H_2O network of the C_0 hydrate by pumping out a gas emitted by metastable recovered C_0 samples at $T = 77-130$ K.[8,10] It was suggested to name the resulting empty H_2O network of the C_0 hydrate "ice XVII".[10] The H_2O molecules in the hexagonal crystal structure of ice XVII form pentagonal rings, which in turn form infinite open helical channels along the *z* axis, as shown in red at the left in Figure 1. The structure possesses chirality, and the space group of ice XVII is $P6_122$ or $P6_522$, depending on the chiral direction.[11−13] Because the diffraction does not distinguish between the enantiomorphic space groups, $P6_122$ could be chosen as an exact space group of ice XVII for convenience.

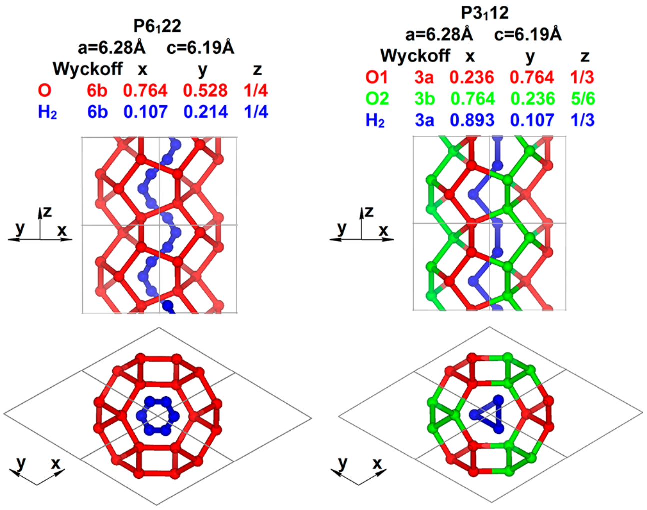

Figure 1. Comparison of the $P6_122$ (left)[13] and $P3_112$ (right)[8,14] structural models for the C_0 hydrate in the H_2O-H_2 system. Oxygen positions and hydrogen bonds for the host H_2O sublattice (ice XVII) are shown by red and green, and the chains of guest H_2 molecules are shown by blue. For clarity, only one resulting helical channel is shown, with the rest being obtained by elementary translations corresponding to a unit cell, shown in gray. The shortest H_2-H_2 intermolecular distances, also shown in blue, are 1.55 and 2.88 Å for the left and right structural models, respectively.

Theoretical calculations[14,15,12] and in situ neutron diffraction experiments on the C_0 hydrate in the D_2O-D_2 system[13] demonstrated that the guest molecules (blue spheres at the left of Figure 1) form one-dimensional spirals inside the helical channels around the 6_1 screw axis. If the 6_122 space group is assumed for the full crystal structure of the C_0 hydrate, including guest H_2 molecules, the resulting distance between the neighbor positions of the guest molecules would be about 1.55 Å. This value is unusually low comparing to the sII,[17] C_1 and C_2 hydrogen hydrates,[3] where the H_2-H_2 distances are about 2.9, 3.0, and 2.3 Å respectively. Thus, a blocking effect should occur between the neighbor H_2 positions in the $P6_122$ crystal structure of the C_0 hydrate, effectively emptying the adjacent positions around each H_2 molecule. This consideration imposes an upper bound of 0.5 on the occupation factor for such position type, limiting the composition $X_{C_0} \leq 0.5$ of the C_0 hydrate.[14,10,11] Also, as the composition approaches its maximum allowed by crystal chemistry value, a long-range order should develop in the arrangement of the guest H_2 molecules. Instead of all H_2 positions being occupied with the same 50% probability, an alternating pattern of empty and occupied sites should develop, resulting in a symmetry breaking. The corresponding scenario of the guest molecule ordering was proposed,[8,14] and the resulting crystal structure is depicted at the right of Figure 1.

Regretfully, the hydrogen content of the C_0 hydrate cannot be determined by direct thermal desorption measurement on recovered samples, because, first, a considerable part of H_2 desorbs during pressure release even at liquid nitrogen temperature[8,10] and, second, when the C_0 hydrate is stored in liquid nitrogen the N_2 molecules are absorbed.[14,10] At present, several different routes were employed to determine the H_2/H_2O content of this hydrate. A lower bound $X_{C_0} \geq 0.13$ was imposed by thermal desorption of quenched and recovered samples.[8] Ab initio[15] and molecular dynamics[14] calculations, performed for fixed $X_{C_0} = 0.5$, demonstrated the stability of the C_0 hydrate with respect to other possible hydrates. A value of $X_{C_0} \approx 0.25$ was reported for the freshly quenched sample as estimated by the intensity ratio of the H_2 and H_2O Raman bands, and X_{C_0} values as high as 0.4 or even 0.5 were reported for ice XVII refilled with hydrogen at the low pressure−low temperature conditions.[10] A composition of $D_2/D_2O = 0.5$ of the C_0 hydrate in the D_2O-D_2 system was determined by in situ neutron diffraction measurements.[13] The accuracies of these values can hardly be estimated, but are unlikely to exceed 10%.

If the H_2/H_2O content of the C_0 hydrate is indeed close to 0.5, then the structural model for this hydrate should have a lower symmetry than that of ice XVII. Thus, an accurate composition determination of the C_0 hydrate is essential for the characterization of its full crystal structure.

Because of the difficulties in the X_{C_0} determination mentioned above, it could be reliably determined only by in situ methods. Volumetry is one of such methods, which has the advantage of being model-independent, and which proved its usefulness in a series of similar problems.[7,8,18]

Our previous efforts to determine the hydrogen content of the phases at the nonvariant quadruple Q_2 point at $P = 3.6$ kbar and $T = +1$ °C[7] were made before the C_0 hydrate was discovered. It was incorrectly assumed that the Q_2 point represents the "sII hydrate + C_1 hydrate + liquid H_2O + H_2 gas" equilibrium,[7] instead of the correct "sII hydrate + C_0 hydrate + liquid H_2O + H_2 gas" one,[8] and the molar volume of the C_1 hydrate was used in the calculations instead of the correct C_0 one, resulting in inaccurate hydrate compositions. In present paper we reconsider the hydrogen content of the phases at equilibrium at the Q_2 point, following the discovery of the correct nature of this point.

In present paper, we also employed in situ volumetry to construct the $C_0 \leftrightarrow C_1$ equilibrium line, and to determine the volume change at this phase transition. Given this volume change, we calculated the composition of the C_0 and C_1 hydrates at their equilibrium from thermodynamical considerations.

2. EXPERIMENTAL DETAILS

The piston−cylinder high-pressure chamber,[19] used for in situ volumetry, is schematically depicted in Figure 2. The loading procedure consisted of several steps. First the device was cooled to about −20 °C via an external thermostat. The double distilled water was frozen and powdered in an agate mortar under liquid nitrogen temperature. The ice sample weighting typically 1−2 g was put in a bronze ampule (3), weighed, and put into the shaft

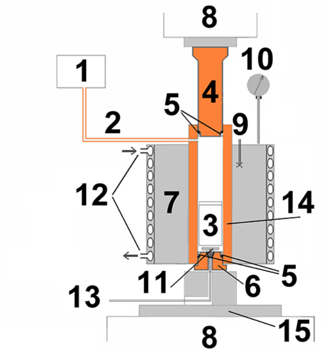

Figure 2. PVT apparatus for in situ high-pressure volumetry: 1, gas compressor up to 1.5 kbar; 2, beryllium bronze capillary; 3, bronze capsule with sample; 4, movable beryllium bronze piston; 5, composite conical sealings, consisting of rubber and bronze O-rings; 6, bottom plug with current leads (not shown is an external housing, restricting the backward movement of the plug); 7, steel support; 8, hydraulic ram; 9, platinum resistive temperature sensor; 10, micrometer gauge for chamber displacement measurement with respect to piston 4; 11, manganin four-probe resistive pressure gauge; 12, cooling jacket with inlets (external thermal insulation is not shown); 13, resistance measurement circuit (not shown); 14, beryllium bronze inner cylinder; 15, thermal insulation.

of the high-pressure vessel with an inner diameter of 12.2 mm and a usable volume of about 10 cm^3. Hydrogen gas of 99.999% purity was supplied at a pressure of about 1.5 kbar by a gas compressor (1) via a beryllium bronze capillary (2). Further gas compression was realized by movement of the beryllium bronze piston (4), which cut off the external gas supply (2) and effectively kept the total hydrogen amount in the high-pressure chamber constant. Hydrogen was always in excess, serving both as a reagent and as a pressure transmitting medium. For clarity, we omit the H_2 subscript hereafter, using P instead of P_{H_2}. The chamber movement with respect to the upper piston was measured with an accuracy of ±0.01 mm by using a micrometer (10), which gave the overall accuracy of about ±0.1 mm^3 of the volume change (absolute volume cannot be determined in present setup). The temperature of the vessel was stabilized to an accuracy of ±0.5 °C, and measured by the resistance sensor (9). The pressure inside the chamber was measured by a four-probe manganin resistance gauge (11). The sensitivities of each used gauge were calibrated in a separate high-pressure chamber, being typically $dR/(R_0\,dP) = 2.41{-}2.46 \times 10^{-6}$ bar^{-1}. The temperature correction of the manganin gauge resistance was measured at ambient pressure in the temperature range between −20 and +55 °C, resulting in a maximal pressure correction of $\Delta P(-20\ °C) = +700$ bar. The gauge resistance was about $R_0 = 100\ \Omega$, which, given the ±0.002 Ω accuracy of resistance measurement, gave the overall pressure sensitivity of 10 bar. Pressure irreproducibility, caused by an irreversible change in R_0 at the end of the experiment, was typically about 100 bar.

The second loading step consisted of ice exposition to a hydrogen pressure of $P = 1.5{-}2$ kbar at $T = -20$ °C for 0.5 h, which was necessary for the complete ice $I_h \rightarrow$ sII hydrate transformation.[7] At the third step, a pressure of $P = 4{-}7$ kbar and temperature of $T = -20$ to +18 °C were reached in the chamber, allowing the C_0 hydrate to form and to equilibrate with the surrounding gas.[7] When no significant pressure drop was detected during 0.5 h, we assumed the sII → C_0 transformation to be complete and proceeded with volumetry measurements. This also ensured the absence of gas leakages, which could otherwise dramatically affect the volumetry results.

3. RESULTS AND DISCUSSION

3.1. The $C_0 \leftrightarrow C_1$ Phase Transition and the Corresponding Volume Change. We constructed the compression and decompression $V(P)$ isotherms, and the $P(T)$ isochores at heating. The isotherms were used to locate the $C_0 \leftrightarrow C_1$ phase equilibrium and to measure the corresponding volume change, and the isochores were used to construct the melting lines of the corresponding hydrates.

The isotherms were constructed via a stepwise piston displacement, followed by a 2−3 min sample equilibration. In the absence of phase transformations, the pressure drift was smaller than 10 bar during that time, and after that we proceeded to the next point. If a phase transformation has started, which manifested itself in a higher pressure drift, we waited until the pressure drift rate dropped below 10 bar per 2−3 min before further piston displacement. The pressures of the $C_0 \rightarrow C_1$ and $C_1 \rightarrow C_0$ phase transformations were assumed to be respectively the lowest and the highest pressures after phase transition onset. The volume changes were determined at these very pressures.

Typical compression−decompression isotherms are shown in Figure 3. The systematical shift between these isotherms is probably explained by an uncontrollable displacement (a backlash) of a bottom plug ((6) in Figure 2) at the first moment of the decompression process.

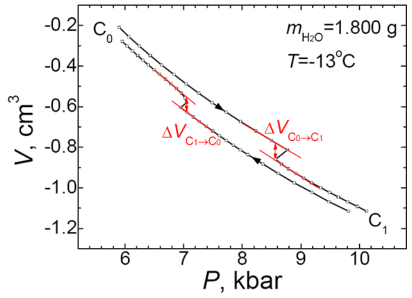

Figure 3. Typical compression and decompression isotherms in the H_2O-H_2 system near the $C_0 \leftrightarrow C_1$ phase transition. The red lines show linear fits to the $V(P)$ dependencies near the transitions, and the red arrows indicate volume changes at the corresponding pressures. Absolute volume value is arbitrary.

A summary of the measured volume changes is presented in Table 1.

The conditions of the $C_0 \rightarrow C_1$ and $C_1 \rightarrow C_0$ phase transitions are shown by the filled and open triangles respectively in Figure 4. The $C_0 \leftrightarrow C_1$ phase transformation is accompanied by a large baric hysteresis, similar to the $I_h \leftrightarrow$ sII and sII $\leftrightarrow C_0$ transformations, studied earlier.[6,7] Because the formation of the C_1 and C_0 phases occurs inside the stability fields of the respective phases, the $C_0 \leftrightarrow C_1$ equilibrium curve, which separates these two stability fields, should also separate the experimental points of the $C_0 \rightarrow C_1$ phase transformation from the points of the reverse one.

We observed the following indications that the hysteresis of the $C_0 \leftrightarrow C_1$ transformation is asymmetric, and the $C_1 \rightarrow C_0$ phase transition is closer to equilibrium:

(1) The points of forward $C_0 \rightarrow C_1$ transformation have much larger scatter (see Figure 4).

Table 1. Volume Changes at the $C_0 \rightarrow C_1$ and $C_1 \rightarrow C_0$ Phase Transitions, Observed at the $V(P)$ Compression and Decompression Isotherms

transition	P, kbar	T, °C	ΔV, $cm^3/mol\ H_2O$
$C_0 \rightarrow C_1$	8.43	7	−1.11
$C_1 \rightarrow C_0$	7.30	7	0.76
$C_0 \rightarrow C_1$	8.60	18	−0.94
$C_1 \rightarrow C_0$	7.19	18	0.80
$C_0 \rightarrow C_1$	8.09	13	−1.02
$C_1 \rightarrow C_0$	7.37	13	0.74
$C_0 \rightarrow C_1$	8.57	−13	−0.86
$C_1 \rightarrow C_0$	7.05	−13	0.74
$C_0 \rightarrow C_1$	9.62	−20	−1.01
$C_1 \rightarrow C_0$	7.24	−20	0.79
$C_0 \rightarrow C_1$	7.91	−3	−0.92

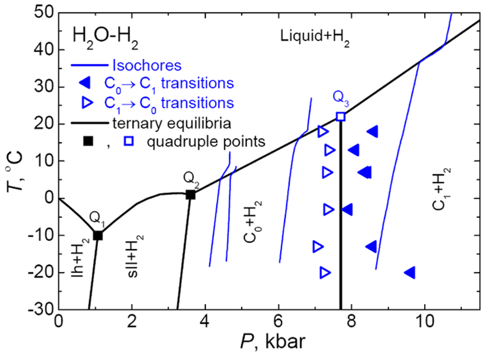

Figure 4. Phase diagram of H_2O under high hydrogen pressure. The black curves show the ternary equilibria, and the triangles show the conditions of the phase transformations, presently observed at the $V(P)$ isotherms. The blue curves are the $P(T)$ isochores at heating. The solid squares show the Q_1 and Q_2 nonvariant quadruple points.[4,7] The open square shows the Q_3 quadruple point, located in present work.

(2) During the cycling $C_0 \rightarrow C_1 \rightarrow C_0 \rightarrow C_1$, the pressure of forward transition at the second pass was significantly lower than that in the first one.

(3) Once started, the forward $C_0 \rightarrow C_1$ transformation proceeded at more or less constant speed, as monitored by a pressure decrease, until it is complete. Accordingly, the slowdown of the observed pressure decrease rate was associated with the transformation end. The reverse transformation demonstrated different behavior: once started, it slowed down quickly, and continued only after further piston displacement.

We drew the equilibrium $C_0 \leftrightarrow C_1$ line at the phase diagram (Figure 4) so that it was closer to the $C_1 \rightarrow C_0$ transformation points. Within experimental uncertainty, this line has a slope of $\left(\frac{dT}{dP}\right)_{C_0 \leftrightarrow C_1} = \infty$ and is located at $P = 7.7(3)$ kbar.

To construct the melting curves of solid phases, we performed the $P(T)$ isochore measurements by heating the high-pressure chamber at a constant rate typically about 5–10 min/°C. The resulting isochores are shown in Figure 4 by the blue curves. Assuming the melting process to proceed without significant overheating, we drew the melting curve of the C_0 hydrate so that it passed through the Q_2 nonvariant quadruple point located previously[7] at $P = 3.6$ kbar and $T = +1$ °C, and through the onsets of melting at the isochores. The resulting curve has a slope of $\left(\frac{dT}{dP}\right)_{C_0 \leftrightarrow L} = 5.5(5)$ K/kbar at Q_2, close to the previous estimate 6.5 K/kbar,[7] and intersects with the $C_0 \leftrightarrow C_1$ line at the Q_3 nonvariant quadruple point at $P = 7.7(3)$ kbar and $T = +22(2)$°C, as shown in Figure 4 by the open square. Having this point located, we drew the melting curve of the C_1 hydrate through this point and the kink at the rightmost isochore in Figure 4. The slope of the C_1 hydrate melting curve was found to be $\left(\frac{dT}{dP}\right)_{C_1 \leftrightarrow L} = 6.8(5)$ K/kbar and that of the C_0 hydrate was $\left(\frac{dT}{dP}\right)_{C_0 \leftrightarrow L} = 5.0(5)$ K/kbar at Q_3.

No statistically important correlation was observed between the T and $\Delta V_{C_0 \leftrightarrow C_1}$ values given in Table 1. A fit of the $\Delta V_{C_0 \leftrightarrow C_1}$ values with a linear function of P gives $\Delta V_{C_0 \rightarrow C_1} = -0.89(5)$ $cm^3/mol\ H_2O$ at 7.7 kbar.

3.2. Volume and Entropy Changes at the Hydrate Melting. *3.2.1. The Q_2 Point.* This quadruple point was located in our previous work[7] at $P = 3.6$ kbar and $T = +1$ °C, where it was incorrectly identified as the "sII hydrate + C_1 hydrate + liquid H_2O + H_2 gas" quadruple point. The volume change, accompanying the sII → C_0 transition, was measured to be $\Delta V_{sII \rightarrow C_0} = -2.01(3)$ $cm^3/mol\ H_2O$.

The difference in the hydrogen content of two phases is determined by a volume change, accompanying the phase transition between them. To determine the absolute value of the hydrogen content of one phase, one should know, however, the content of the other. In this paper, we rely on the absolute value of X_L, estimated in section 3.3.

The volume changes corresponding to the liquid → hydrate phase transformations could hardly be measured, because these phase transformations are accompanied by a large overcooling of about 20° and simultaneous formation of metastable gas-poor high-pressure ices, so that single-phase state of the sample could never be reached then.[20] Fortunately, these volume changes can be calculated provided the $\frac{dT}{dP}$ slopes of ternary equilibria curves were established. The curves of the sII ↔ L, sII ↔ C_0, and L ↔ C_0 equilibria were constructed in the pressure–temperature phase diagram of the system,[7] and their slopes were estimated as $\left(\frac{dT}{dP}\right)_{sII \leftrightarrow C_0} = 89$ K/kbar, $\left(\frac{dT}{dP}\right)_{C_0 \leftrightarrow L} = 6.5$ K/kbar and $\left(\frac{dT}{dP}\right)_{L \leftrightarrow sII} = -1.5$ K/kbar at Q_2. In present study, we reconsider $\left(\frac{dT}{dP}\right)_{C_0 \leftrightarrow L} = 5.5(5)$ K/kbar (see previous section).

The slopes of the equilibrium curves in a pressure–temperature phase diagram of a binary system are known to follow the Clausius–Clapeyron relations,[21] which allows us to construct the conditions of self-consistency around Q_2 point:

$$\left(\frac{dT}{dP}\right)_{sII \leftrightarrow C_0} = \frac{\Delta V_{sII \rightarrow C_0}}{\Delta S_{sII \rightarrow C_0}}$$

$$\left(\frac{dT}{dP}\right)_{C_0 \leftrightarrow L} = \frac{\Delta V_{C_0 \rightarrow L}}{\Delta S_{C_0 \rightarrow L}}$$

$$\left(\frac{dT}{dP}\right)_{L \leftrightarrow sII} = \frac{\Delta V_{L \rightarrow sII}}{\Delta S_{L \rightarrow sII}}$$

$$\Delta V_{sII \rightarrow C_0} + \Delta V_{C_0 \rightarrow L} + \Delta V_{L \rightarrow sII} = 0$$

$$\Delta S_{sII \rightarrow C0} + \Delta S_{C_0 \rightarrow L} + \Delta S_{L \rightarrow sII} = 0 \qquad (1)$$

The results of solving this system of equations with respect to unknown variables is shown in Table 2 below:

Table 2. Volume and Entropy Changes, Accompanying the Phase Transformations near the Q_2 point (P = 3.6 kbar, T = +1°C)

transition	ΔV, $cm^3/mol\ H_2O$	ΔS, J/(K mol H_2O)
sII → C_0	−2.01(3)	−2.26(3)
C_0 → L	1.61(5)	29(2)
L → sII	0.40(5)	−27(2)

3.2.2. The Q_3 Point.

Present experimental data suggest that the Q_3 point is located at $P = 7.7(3)$ kbar and $T = +22(2)$°C. The slopes of the phase equilibria curves which meet at Q_3 are $\left(\frac{dT}{dP}\right)_{C_0\leftrightarrow C_1} = \infty$, $\left(\frac{dT}{dP}\right)_{C_1\leftrightarrow L} = 6.8(5)$ K/kbar and $\left(\frac{dT}{dP}\right)_{L\leftrightarrow C_0} = 5.0(5)$ K/kbar. Taking into account the experimental volume change $\Delta V_{C_0\rightarrow C_1} = -0.89(5)\ cm^3/mol\ H_2O$ (see section 3.1), it is possible to compose and solve the self-consistency conditions for the Q_3 point in analogy to eq 1. The result of solving the system of equations with respect to unknown variables is shown in Table 3 below:

Table 3. Volume and Entropy Changes, Accompanying the Phase Transformations near the Q_3 point (P = 7.7(3) kbar and T = +22(2)°C)

transition	ΔV, $cm^3/mol\ H_2O$	ΔS, J/(K mol H_2O)
C_0 → C_1	−0.89(5)	0
C_1 → L	3.4(10)	50(15)
L → C_0	−2.5(10)	−50(15)

3.3. Hydrogen Solubility in Liquid H_2O.

To estimate the hydrogen content X_{C_0} and X_{C_1} of the C_0 and C_1 hydrates, the pressure dependence of the equilibrium hydrogen solubility in a liquid X_L should be characterized first. Then, the volume changes at hydrate melting, estimated in the previous section, can be used to determine $\Delta X_{L\rightarrow C_0}$ and $\Delta X_{L\rightarrow C_1}$.

Hydrogen solubility in liquid water was measured[22] up to 1 kbar for temperatures from 0−100 °C. The maximal observed solubility was about $X_L = \frac{H_2}{H_2O} \approx 0.015$. The rest of this section discusses an extrapolation of the hydrogen solubility in water up to high pressures of 8 kbar.

The equation of state for pure water was accurately measured in the pressure range of interest,[23] as shown by the black curve in Figure 5. Hydrogen dissolution in water causes volume expansion of $\beta = \partial V_L/\partial X_L = 26\ cm^3/mol\ H_2$.[24,25] Regretfully, no studies of pressure dependence of β were published up to date. To model the pressure dependence of β we assumed the ratio of β to the molar volume of hydrogen-free water $V_L^{H_2O}$ to be pressure-independent. Equivalently, the bulk modulus of hydrogen solution in water is assumed to be independent from its hydrogen content X_L. The $\beta(P)$ dependence obtained in this way is shown by the red curve in Figure 5.

According to the equation of state of hydrogen gas[26] (the green curve in Figure 5), at pressures higher than 3 kbar, the hydrogen molar volume $V_{gas}^{H_2}$ becomes smaller than β, and the overall ΔV for the reaction

$$H_2O(\text{liquid}) + X_L H_2 \rightarrow H_2O \times X_L H_2(\text{solution}) \qquad (2)$$

becomes positive. Thus, further hydrogen pressure increase destabilizes hydrogen solution in water according to le Chatelier's principle. The equilibrium $X_L(P)$dependence has a maximum at about 3 kbar and a decrease at higher pressures.

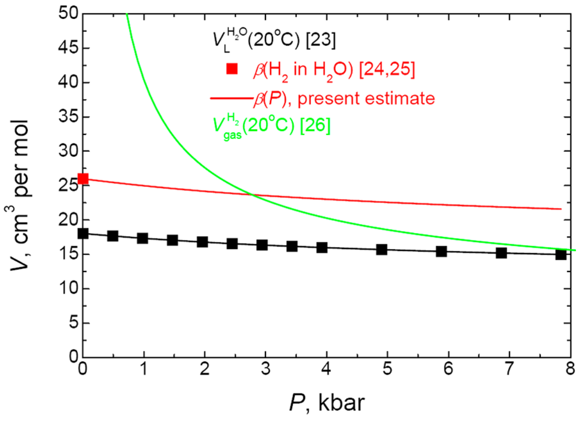

Figure 5. Pressure dependence of the molar volumes for liquid H_2O (black symbols and curve)[23] and hydrogen gas (green curve),[26] volume expansion β of liquid H_2O caused by hydrogen dissolution in it at ambient pressure (red square),[24,25] and present estimate of the $\beta(P)$ dependence (red curve).

Consider the Gibbs energy $G(X_L, P)$ for the reaction (eq 2) as a function of X_L at certain pressure P and fixed temperature. An equilibrium value of $X_L(P)$ corresponds to a minimum of such G. Assuming that the $G(P_0)$ is known for any X_L, the $G(P)$ can be constructed at particular pressure: $G(P) = G(P_0) + X_L \int_{P_0}^{P} \beta(P) - V_{gas}^{H_2}(P)\, dP$. Note that $X_L(P)$ can be in principle determined unambiguously provided that the $G(P_0)$ is known for any X_L, and given the value of $\int_{P_0}^{P} \beta(P) - V_{gas}^{H_2}(P)\, dP$. Particularly, if $\int_{P_1}^{P_2} \beta(P) - V_{gas}^{H_2}(P)\, dP = 0$ at certain pressures P_1 and P_2, then $X_L(P_1) = X_L(P_2)$.

Would the solution be diluted, its Gibbs free energy would be $G(P_0) = \text{const}\, X_L + RTX_L \ln X_L$, and the equilibrium solubility $X_L(P) = \text{const}\, \exp(\int_{P_0}^{P} V_{gas}^{H_2}(P) - \beta(P)\, dP/RT)$ can be derived from the condition $\frac{\partial G(P)}{\partial X_L} = 0$.

To extrapolate the literature data[22] for hydrogen solubility in liquid H_2O to higher pressures, we plotted $X_L(P)$ against $P_0 \exp(\int_{P_0}^{P} V_{gas}^{H_2} - \beta\, dP/RT)$, as shown at the left of Figure 6. The nonlinearity of these plots is a manifestation of the nonideal

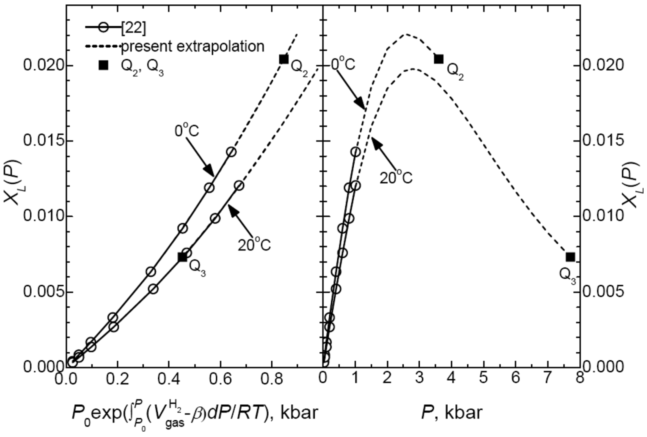

Figure 6. Literature data for hydrogen solubility in liquid H_2O (open circles and solid curves)[22] and present extrapolation to higher pressures (dashed curves and squares).

DOI: 10.1021/acs.jpcc.8b12083
J. Phys. Chem. C 2019, 123, 3696−3702

behavior of hydrogen solution in liquid H_2O. It should be noted that the dependence of $P_0 \exp(\int_{P_0}^{P} V_{\mathrm{gas}}^{\mathrm{H_2}} - \beta \, \mathrm{d}P/RT)$ as well as X_{L} on P is nonmonotonic: both quantities reach a maximum at about $P \approx 3$ kbar, and both decrease at higher pressures. In general, each value of $P_0 \exp(\int_{P_0}^{P} V_{\mathrm{gas}}^{\mathrm{H_2}} - \beta \, \mathrm{d}P/RT)$ as well as X_{L} results from two different values of P — one above and one below the maximum solubility pressure. Thus, the curves shown at the left of Figure 6 pass through each point on the plot two times. Because both $P(\mathrm{Q_2})$ and $P(\mathrm{Q_3})$ are above the pressures of maximal hydrogen solubility in water, these points appear on the plot at the second pass on the respective curves. The corresponding X_{L} dependencies on P at $T = 0$ and 20 °C are shown at the right of Figure 6. Based on these dependencies, we estimated $X_{\mathrm{L}}(\mathrm{Q_2}) \approx 0.020$ and $X_{\mathrm{L}}(\mathrm{Q_3}) \approx 0.007$.

The volume of pure liquid H_2O without hydrogen at the conditions of $\mathrm{Q_2}$ quadruple point is $V_{\mathrm{L}}^{\mathrm{H_2O}}(\mathrm{Q_2}) = 16.00$ cm^3/mol H_2O.[23] The volume of saturated hydrogen solution in liquid can be estimated as $V_{\mathrm{L}}(\mathrm{Q_2}) = V_{\mathrm{L}}^{\mathrm{H_2O}} + X_{\mathrm{L}}\beta = 16.46$ cm^3/mol H_2O. The respective volumes at $\mathrm{Q_3}$ are $V_{\mathrm{L}}^{\mathrm{H_2O}}(\mathrm{Q_3}) = 15.04$ cm^3/mol H_2O and $V_{\mathrm{L}}(\mathrm{Q_3}) = 15.20$ cm^3/mol H_2O.

We will now introduce a "reduced volume" $V_{\mathrm{L}}^{-\mathrm{H}}$ for a liquid saturated with gas as following: $V_{\mathrm{L}}^{-\mathrm{H}} = V_{\mathrm{L}} - X_{\mathrm{L}} V_{\mathrm{gas}}^{\mathrm{H_2}}$, with analogous definition for all solid phases. The total volume change during the phase transformation between the two phases, which can be measured experimentally by volumetry, is equal to the difference of their reduced volumes, e.g., $\Delta V_{\mathrm{L}\to\mathrm{sII}} = V_{\mathrm{sII}}^{-H} - V_{\mathrm{L}}^{-\mathrm{H}}$ and so on.

Using the values $V_{\mathrm{gas}}^{\mathrm{H_2}}(\mathrm{Q_2}) = 20.72$ cm^3/mol H_2 and $V_{\mathrm{gas}}^{\mathrm{H_2}}(\mathrm{Q_3}) = 15.90$ cm^3/mol H_2 from the literature equation of state of H_2,[26] the reduced volumes of liquid are evaluated at $\mathrm{Q_2}$ and $\mathrm{Q_3}$: $V_{\mathrm{L}}^{-\mathrm{H}}(\mathrm{Q_2}) = V_{\mathrm{L}} - X_{\mathrm{L}} V_{\mathrm{gas}}^{\mathrm{H_2}} = 16.05$ cm^3/mol H_2O and $V_{\mathrm{L}}^{-\mathrm{H}}(\mathrm{Q_3}) = 15.09$ cm^3/mol H_2O.

3.4. Hydrogen Content of the Hydrates. Using the reduced volume of a liquid, calculated in the previous section, and given the volume changes accompanying the melting of hydrates, obtained in sections 3.2.1 and 3.2.2, it is straigtforward to compute the reduced volumes of hydrates: $V_{\mathrm{sII}}^{-\mathrm{H}} = V_{\mathrm{L}}^{-\mathrm{H}} + \Delta V_{\mathrm{L}\to\mathrm{sII}} = 16.5$ cm^3/mol H_2O and $V_{\mathrm{C_0}}^{-\mathrm{H}} = V_{\mathrm{L}}^{-\mathrm{H}} - \Delta V_{\mathrm{C_0}\to\mathrm{L}} = 14.5$ cm^3/mol H_2O at $\mathrm{Q_2}$; $V_{\mathrm{C_0}}^{-\mathrm{H}} = V_{\mathrm{L}}^{-\mathrm{H}} + \Delta V_{\mathrm{L}\to\mathrm{C_0}} = 12.6$ cm^3/mol H_2O and $V_{\mathrm{C_1}}^{-\mathrm{H}} = V_{\mathrm{L}}^{-\mathrm{H}} - \Delta V_{\mathrm{C_1}\to\mathrm{L}} = 11.7$ cm^3/mol H_2O at $\mathrm{Q_3}$.

The molar volume of sII hydrate at $\mathrm{Q_2}$ $V_{\mathrm{sII}} = 21.77$ cm^3/mol H_2O was obtained earlier[7] by extrapolation of in situ X-ray and neutron diffraction data.[5,6,17] Thus, the content of the sII hydrate at $\mathrm{Q_2}$ is $X_{\mathrm{sII}}(\mathrm{Q_2}) = (V_{\mathrm{sII}} - V_{\mathrm{sII}}^{-\mathrm{H}})/V_{\mathrm{H_2}}^{\mathrm{gas}} = 0.26(2)$. This value is considerably less than the maximal allowed by crystal chemistry value $X_{\mathrm{sII}}^{\mathrm{max}} = 48/136 \approx 0.353$, and also somewhat less than the previous estimate $X_{\mathrm{sII}}(\mathrm{Q_2}) = 0.32$,[7] based on incorrect assumptions. Given the earlier estimation of $X_{\mathrm{sII}}(\mathrm{Q_1}) = 0.207(5)$ at the nonvariant $\mathrm{Q_1}$ quadruple point "ice $\mathrm{I_h}$ + sII hydrate + liquid H_2O + H_2 gas" ($P = 1.07$ kbar $T = -10$ °C),[7] it follows that X_{sII} only slightly increases with pressure along the sII hydrate melting line.

To obtain the molar volume of the $\mathrm{C_0}$ hydrate at $\mathrm{Q_2}$ and $\mathrm{Q_3}$, we collected all available data on X-ray and neutron in situ diffaction[9,11,13] at $P = 3{-}7.3$ kbar and $T = -103$ to $+7$ °C. The resulting data set can be fit with a linear dependence $V_{\mathrm{C_0}}$ [cm^3/mol H_2O] = 21.60−0.07P [kbar] + 0.002T [°C], which gives $V_{\mathrm{C_0}}(\mathrm{Q_2}) = 21.35$ cm^3/mol H_2O and $V_{\mathrm{C_0}}(\mathrm{Q_3}) = 21.10$ cm^3/mol H_2O. The corresponding hydrogen content of the $\mathrm{C_0}$ phase at $\mathrm{Q_2}$ is $X_{\mathrm{C_0}}(\mathrm{Q_2}) = (V_{\mathrm{C_0}} - V_{\mathrm{C_0}}^{-\mathrm{H}})/V_{\mathrm{gas}}^{\mathrm{H_2}} = 0.33(2)$, and at $\mathrm{Q_3}$ it is $X_{\mathrm{C_0}}(\mathrm{Q_3}) = 0.53(5)$. One can see that the hydrogen content of the $\mathrm{C_0}$ hydrate considerably depends on the $P{-}T$ conditions, particularly, at $\mathrm{Q_2}$ the hydrogen content is considerably less than the maximal allowed value $X_{\mathrm{C_0}}^{\mathrm{max}} = 1/2$. When compared to the literature data[13] $X_{\mathrm{C_0}}(0.3\ \mathrm{GPa}, 175\ \mathrm{K}) = 1/2$, it follows that $X_{\mathrm{C_0}}$ considerably depends on temperature.

We also collected all available XRD data for the $\mathrm{C_1}$ hydrate[3,27,9] and linearly fit them with the following equation: $V_{\mathrm{C_1}}$ [cm^3/mol H_2O] = 15.94−0.09P [kbar] + 0.001T [°C], which gave us $V_{\mathrm{C_1}}(\mathrm{Q_3}) = 15.30$ cm^3/mol H_2O. The hydrogen content of the $\mathrm{C_1}$ hydrate at the $\mathrm{Q_3}$ point can be calculated then: $X_{\mathrm{C_1}}(\mathrm{Q_3}) = (V_{\mathrm{C_1}} - V_{\mathrm{C_1}}^{-\mathrm{H}})/V_{\mathrm{gas}}^{\mathrm{H_2}} = 0.23(5)$. Because this value is close to the maximal one allowed by crystal chemistry $X_{\mathrm{C_1}}^{\mathrm{max}} = 1/6 \approx 0.167$, it follows that the $\mathrm{C_1}$ hydrate, unlike the sII and $\mathrm{C_0}$ hydrates, is a nearly stoichiometric compound. This result agrees with our previous estimate of the $\mathrm{C_1}$ hydrate hydrogen content from 1.5 to 2 wt % ($X_{\mathrm{C_1}} = 0.13{-}0.18$), measured by thermal desorption on the samples quenched at 20 kbar,[28,8] and with the Raman-based estimate $X_{\mathrm{C_1}} = 0.1{-}0.2^3$.

The results on individual phases are summarized in Tables 4 and 5.

Table 4. Equilibrium Compositions and Molar Volumes of Different Phases in the $H_2O{-}H_2$ System at the $\mathrm{Q_2}$ Point

phase	X	V, cm^3/mol H_2O
liquid	0.02(1)	16.46
sII	0.26(2)	21.77
$\mathrm{C_0}$	0.33(2)	21.35
H_2 gas	∞	20.72

Table 5. Equilibrium Compositions and Molar Volumes of Different Phases in the $H_2O{-}H_2$ System at the $\mathrm{Q_3}$ Point

phase	X	V, cm^3/mol H_2O
liquid	0.01(1)	15.20
$\mathrm{C_0}$	0.53(5)	21.10
$\mathrm{C_1}$	0.23(5)	15.30
H_2 gas	∞	15.90

The dependence of the hydrogen content of hydrates on pressure along their melting line is shown in Figure 7.

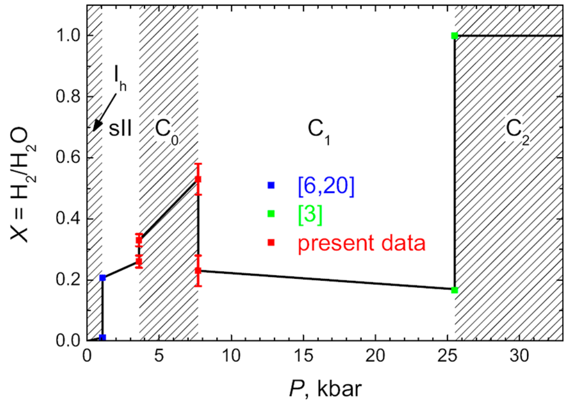

Figure 7. Hydrogen content of solid phases in the $H_2O{-}H_2$ system along their melting lines as a function of hydrogen pressure. Present estimates are shown by the red squares.

DOI: 10.1021/acs.jpcc.8b12083
J. Phys. Chem. C 2019, 123, 3696−3702

4. CONCLUSIONS

We performed in situ volumetric study of H_2O under high hydrogen pressure up to 10 kbar, effectively completing the construction of the H_2O-H_2 phase diagram in this pressure range (Figure 4). The obtained volumetric data are used to determine the $\frac{dT}{dP}$ slopes of the phase transformations of the C_0 hydrogen hydrate to the neighbor phases, and also volume and entropy changes, accompanying these transformations (Tables 2 and 3).

The literature data were analyzed to obtain the molar volumes of the C_0 and C_1 hydrates at their equilibrium, which, combined with our volumetric data, allowed us to reliably determine the hydrogen content of these hydrates near quadruple points along their melting curve (Table 5 and Figure 7).

The composition of the C_0 hydrate, similar to that of the sII hydrate, considerably depends both on pressure and temperature. Along the melting curve, $X_{C_0} = \frac{H_2}{H_2O}$ changes from 0.33(2) (Table 4) to the nearly stoichiometric value 0.53(5) ≈ 1/2 (Table 5). At such high X_{C_0}, the hydrogen molecules in the C_0 phase should be ordered, which supports the trigonal crystal structure of this phase suggested earlier.[8,14]

The composition of the C_1 hydrate is found to be X_{C_1} = 0.23(5) at its lower pressure of stability (Table 5), which is close to the stoichiometric value $X_{C_1} = 1/6$, reported in the literature[3] for this phase at its highest pressure of stability. This suggests that the C_1 hydrate has nearly constant composition within its stability field (Figure 7).

AUTHOR INFORMATION

Corresponding Author

*E-mail: kuz@issp.ac.ru.

ORCID

M. A. Kuzovnikov: 0000-0003-4030-4861

Notes

The authors declare no competing financial interest.

ACKNOWLEDGMENTS

The work was supported by the Program "Physics of Fundamental Interactions and Nuclear Technologies" of the Russian Academy of Sciences.

REFERENCES

(1) Levi, A.; Kenyon, S. J.; Podolak, M.; Prialnik, D. H-atmospheres of Icy Super-Earths Formed In Situ in the Outer Solar System: An Application to a Possible Planet Nine. *Astrophys. J.* **2017**, *839*, 111.

(2) Koh, C. A.; Sloan, E. D., Jr. *Clathrate Hydrates of Natural Gases*, 3rd ed.; CRC Press, 2007.

(3) Vos, W. L.; Finger, L. W.; Hemley, R. J.; Mao, H. Novel H_2-H_2O Clathrates at High Pressures. *Phys. Rev. Lett.* **1993**, *71* (19), 3150−3153.

(4) Dyadin, Yu. A.; Larionov, E. G.; Manakov, A. Yu.; Zhurko, F. V.; Aladko, E. Ya.; Mikina, T. V.; Komarov, V. Yu. Clathrate Hydrates of Hydrogen and Neon. *Mendeleev Commun.* **1999**, *9* (5), 209−210.

(5) Mao, W. L.; Mao, H.; Goncharov, A. F.; Struzhkin, V. V.; Guo, Q.; Hu, J.; Shu, J.; Hemley, R. J.; Somayazulu, M.; Zhao, Y. Hydrogen Clusters in Clathrate Hydrate. *Science* **2002**, *297*, 2247−2249.

(6) Efimchenko, V. S.; Antonov, V. E.; Barkalov, O. I.; Beskrovnyy, A. I.; Fedotov, V. K.; Klyamkin, S. N. Phase Transistions and Equilibrium Hydrogen Content of Phases in the Water-Hydrogen System at Pressures to 1.8 kbar. *High Pressure Res.* **2006**, *26*, 439−443.

(7) Antonov, V. E.; Efimchenko, V. S.; Tkacz, M. Phase Transitions in the Water-Hydrogen System at Pressures up to 4.7 kbar. *J. Phys. Chem. B* **2009**, *113*, 779−785.

(8) Efimchenko, V. S.; Kuzovnikov, M. A.; Fedotov, V. K.; Sakharov, M. K.; Simonov, S. V.; Tkacz, M. New Phase in the Water−Hydrogen System. *J. Alloys Compd.* **2011**, *509S*, S860−S863.

(9) Strobel, T. A.; Somayazulu, M.; Hemley, R. J. Phase Behavior of H_2-H_2O at High Pressures and Low Temperatures. *J. Phys. Chem. C* **2011**, *115*, 4898−4903.

(10) del Rosso, L.; Celli, M.; Ulivi, L. New Porous Water Ice Metastable at Atmospheric Pressure Obtained by Emptying a Hydrogen-Filled Ice. *Nat. Commun.* **2016**, *7*, 13394.

(11) Strobel, T. A.; Somayazulu, M.; Sinogeikin, S. V.; Dera, P.; Hemley, R. J. Hydrogen-Stuffed, Quartz-like Water Ice. *J. Am. Chem. Soc.* **2016**, *138*, 13786−13789.

(12) del Rosso, L.; Grazzi, F.; Celli, M.; Colognesi, D.; Garcia-Sakai, V.; Ulivi, L. Refined Structure of Metastable Ice XVII from Neutron Diffraction Measurements. *J. Phys. Chem. C* **2016**, *120*, 26955−26959.

(13) Amos, D. M.; Donnelly, M.-E.; Teeratchanan, P.; Bull, C. L.; Falenty, A.; Kuhs, W. F.; Hermann, A.; Loveday, J. S. A Chiral Gas-Hydrate Structure Common to the Carbon Dioxide-Water and Hydrogen-Water Systems. *J. Phys. Chem. Lett.* **2017**, *8*, 4295−4299.

(14) Smirnov, G. S.; Stegailov, V. V. Toward Determination of the New Hydrogen Hydrate Clathrate Structures. *J. Phys. Chem. Lett.* **2013**, *4*, 3560−3564.

(15) Qian, G.-R.; Lyakhov, A. O.; Zhu, Q.; Oganov, A. R.; Dong, X. Novel Hydrogen Hydrate Structures under Pressure. *Sci. Rep.* **2014**, *4*, 5606.

(16) Smirnov, G. S.; Stegailov, V. V. Anomalous Diffusion of Guest Molecules in Hydrogen Gas Hydrates. *High Temp.* **2015**, *53*, 829−836.

(17) Lokshin, K. A.; Zhao, Y.; He, D.; Mao, W. L.; Mao, H.-K.; Hemley, R. J.; Lobanov, M. V.; Greenblatt, M. Structure and Dynamics of Hydrogen Molecules in the Novel Clathrate Hydrate by High Pressure Neutron Diffraction. *Phys. Rev. Lett.* **2004**, *93*, 125503.

(18) Manakov, A. Y.; Ogienko, A. G.; Tkacz, M.; Lipkowski, J.; Stoporev, A. S.; Kutaev, N. V. High-Pressure Gas Hydrates of Argon: Compositions and Equations of State. *J. Phys. Chem. B* **2011**, *115*, 9564−9569.

(19) Baranowski, B.; Tkacz, M.; Bujnowski, W. Determination of the Absorption/Desorption Isotherms in Metal-Hydrogen Systems at High Pressures. *High Temp.-High Press.* **1976**, *8*, 656−658.

(20) Efimchenko, V. S.; Antonov, V. E.; Barkalov, O. I.; Klyamkin, S. N. Temperature-Pressure Phase Diagram of a D_2O-D_2 System at Pressures to 1.8 kbar. *J. Phys. Chem. B* **2008**, *112*, 7026−7031.

(21) Antonov, V. E.; Sholin, I. A. Proving the Contact Rules for Phase Regions: Implications to Phase Diagrams of Metal-Hydrogen Systems. *J. Alloys Compd.* **2015**, *645*, S160−S165.

(22) Wiebe, R.; Gaddy, V. L. The Solubility of Hydrogen in Water at 0, 50, 75 and 100° from 25 to 1000 Atmospheres. *J. Am. Chem. Soc.* **1934**, *56*, 76−79.

(23) Bridgman, P. W. The Pressure-Volume-Temperature Relations of the Liquid, and the Phase Diagram of Heavy Water. *J. Chem. Phys.* **1935**, *3*, 597.

(24) Moore, J. C.; Battino, R.; Rettich, T. R.; Handa, Y. P.; Wilhelm, E. Partial Molar Volumes of "Gases" at Infinite Dilution in Water at 298.15 K. *J. Chem. Eng. Data* **1982**, *27*, 22−24.

(25) Tiepel, E. W.; Gubbins, K. E. Partial Molal Volumes of Gases Dissolved in Electrolyte Solutions. *J. Phys. Chem.* **1972**, *76*, 3044−3049.

(26) Tkacz, M.; Litwiniuk, A. Useful Equations of State of Hydrogen and Deuterium. *J. Alloys Compd.* **2002**, *330−332*, 89−92.

(27) Hirai, H.; Ohno, S.; Kawamura, T.; Yamamoto, Y.; Yagi, T. Changes in Vibration Modes of Hydrogen and Water Molecules and in Lattice Parameters with Pressure for Filled-Ice Hydrogen Hydrates. *J. Phys. Chem. C* **2007**, *111*, 312−315.

(28) Efimchenko, V. S.; Kuzovnikov, M. A.; Sakharov, M. K.; Tkacz, M. Crystal Structure and Composition of Hydrogen Hydrate C_1. *Proceedings of the ICHMS'2009, Yalta, Crimea, Ukraine, Aug 25−31, 2009*; Schur, D. V., Zaginaichenko, S. Yu., Veziroglu, T. N., Skorokhod, V. V., Eds.; AHEU: Kyiv, pp 220−221.